

Graphene in Strain Sensing Applications

Subjects: [Engineering, Electrical & Electronic](#) | [Instruments & Instrumentation](#) | [Engineering, Mechanical](#)

Contributor: Murat Kaya Yapici

Strain sensors, otherwise known as strain gauges, are fueled by various nanomaterials, among which graphene has attracted great interest in recent years, due to its unique electro-mechanical characteristics. Graphene shows not only exceptional physical properties but also has remarkable mechanical properties, such as piezoresistivity, which makes it a perfect candidate for strain sensing applications.

graphene

strain sensor

strain gauge

gauge factor

piezoresistance

piezoresistivity

MEMS

graphene transfer and integration

1. Introduction

With the advent of the internet-of-things (IoT), smart, ubiquitous, pervasive sensing is rapidly gaining importance for providing reliable information at unprecedented sensitivity to enable new applications in consumer electronics [\[1\]](#) [\[2\]](#)[\[3\]](#), healthcare [\[4\]](#)[\[5\]](#)[\[6\]](#), manufacturing and structural monitoring [\[7\]](#)[\[8\]](#), transportation [\[9\]](#)[\[10\]](#), defense and surveillance [\[11\]](#)[\[12\]](#)[\[13\]](#); as well as to fuel research in fundamental, applied and translational science [\[14\]](#). Among the various physical measurands, the monitoring of strain finds use in numerous applications and industrial products where the fundamental detection principle relies on the change in electrical properties of the strain sensing element as a result of applied pressure or force. Strain sensors essentially rely on four fundamental sensing modalities which are capacitive, piezoelectric, piezoresistive and optical sensing [\[15\]](#). Among these, piezoresistive sensors, with their low-cost-fabrication and easy data analysis advantages, have gathered significant attention.

Typically, sensors based on piezoresistivity rely on transducing external mechanical loading into resistance change, which usually follows a linear relationship [\[16\]](#). Commonly, piezoresistive sensors harness the piezoresistive effect of the sensing material whereby its conductance changes with applied strain, along with change in resistance of the entire sensor assembly due to geometry change upon deformation. To design high-performance piezoresistive sensors, different parameters such as stretchability, sensitivity, dynamic range, limit of detection, accuracy, response speed, stability, durability, fabrication cost and simplicity should be considered. Out of these design criteria, the fundamental figure-of-merit for a strain sensor is its sensitivity, which is evaluated by the gauge factor (GF), formally defined as the ratio of relative resistance change in the sensing element to the mechanical strain acting on it ($GF = \Delta R/R/\epsilon$).

To date, various materials have been investigated for use as strain sensing elements, in an effort to optimize the response of the strain sensor with respect to the attributes mentioned above. Realizing a strain sensor operating at

a wide strain range with good sensitivity has been an especially huge challenge. To overcome the problem of low sensitivity, different approaches have been proposed including doping, defect deformation and exploiting different piezoresistive sensing mechanisms along with sensing materials [17][18][19][20][21].

Among the most typical strain sensing materials are metals. However, strain sensors based on metals, otherwise known as metal-foil gauges, primarily rely on resistance change due to dimensional change of electrically conducting thin lines typically structured in the form of a serpentine, and as such the gauge factors are typically limited to single digits [14][22]. Several other strain sensors with different types of semiconductor piezoresistive materials, including doped polysilicon have also been developed, which offer much higher gauge factors compared to metal-foil counterparts [23].

As an alternative to some of these conventional materials like metals, metal oxides, semiconductors and ceramics which suffer either from intrinsic hardness, brittleness, low strain range or poor scalability, in recent years, carbon-based materials have been on the forefront of “sensor research”, including strain sensing [21][22][23][24][25]. As such, nanomaterials including carbon nanotubes (CNT) and graphene have both been reported as functional materials to realize strain sensors [24]. While CNTs have an almost one-dimensional (1D) structure [25], graphene has an ideal two-dimensional (2D) structure which potentially allows conventional device fabrication by planar, semiconductor process technologies. Additionally, its piezoresistive property [26][27] together with its exceptional physical, electrical [28] and mechanical properties (Young’s modulus on the order of 1 TPa) [29] render graphene an ideal candidate for strain sensors [30].

2. Fundamental Material Properties and Piezoresistive Effect in Graphene

Graphene is a crystalline allotrope of carbon, which consists of a single-layer sheet of sp^2 hybridized carbon atoms. After its exploration in 2004, graphene it has drawn a lot of attention due to its excellent electrical, mechanical, optical and magnetic properties [31][32][33][34][35][36].

2.1. Electrical Properties

Studies on the electronic properties of graphene show that it is a new class of material resembling a zero-bandgap semiconductor and even acting more like a metal, yet still harboring the potential to have a bandgap and Fermi level by various methods, including doping [37]. Electronic properties of graphene also strongly depend on crystallite thickness. In single layer graphene, the band gap is zero, making it behave like a semiconductor or semi-metal, while the multilayer graphene shows metallic behavior as a result of the overlap in carrier wave function, which is due to the multiple graphene layers stacking [38]. The unique band structure of monolayer graphene leads to excellent traits, such as ballistic transport properties and anomalous quantum Hall effects, ultrahigh mobility (200,000 $cm^2/V\cdot s$) and high specific electrical conductivity (SEC) (0.95–1.67 $S m^2/g$) [39], which can vary with applied strain.

Earlier study has shown the effect of the applied strain on opening the band gap of single-crystal graphene at the Fermi level, which results in the decrease of its electrical conductivity [40]. At low energies, graphene contains two linear energy bands that meet at high symmetric points and are isotropic with regard to the points at equilibrium. Effect of different strain types on the electronic properties of graphene reveals that, when isotropic strain is applied, graphene shows electronic properties that are independent of the isotropic strain since the isotropic strain follows crystal symmetries [41]. Strain can be intentionally or naturally imposed on graphene. By bending the substrates on which graphene is extended without slippage, uniaxial strain can be generated. To understand the effect of the uniaxial strain, armchair and zigzag graphene nanoribbons were studied, and they were reported to have different electronic properties. The electronic properties of the zigzag nanoribbons were independent of the uniaxial strain whereas the armchair nanoribbons were predicted to have energy gaps varying with the armchair shape [42].

2.2. Mechanical Properties

Graphene, as a two-dimensional one atomic layer thick material, sustains up to 25% in-plane tensile strain, making it one of the most flexible, uniform, zero band-gap semiconductors [43]. Graphene is known for its very high in-plane stiffness (high Young's modulus), and the highest ever measured mechanical strength [33][44][45]. The 2D breaking strength and elastic stiffness of free-standing monolayer graphene membranes measured by an atomic force microscope (AFM) showed $42 \text{ N}\cdot\text{m}^{-1}$ and $340 \text{ N}\cdot\text{m}^{-1}$, respectively [33]; rendering graphene as the strongest material ever measured. These correspond to near theoretical limits including a mechanical stiffness of 1 TPa and an intrinsic tensile strength of 130 GPa at 25% strain, which are also comparable to in-plane values of graphite and single-walled and multi-walled carbon nanotubes [33]. It is important to note, however, that such mechanical properties largely depend on the testing temperature, sample geometry and even the measurement technique utilized. For instance, a layer of suspended exfoliated graphene located on a trench pattern of silicon oxide/silicon substrate was analyzed with AFM, showing graphene thickness of less than 10 nm, spring constant in the range of 1 to 5 N/m, and Young's modulus of 0.5 TPa, which is less than that of bulk graphite typically ranging around 1 TPa [46]. Overall, the remarkable mechanical properties of graphene are very important, especially for flexible, stretchable electronics and/or wearable applications where robust and functional materials with excellent electronic and structural properties are needed [47].

2.3. Piezoresistivity

A piezoresistive effect is observed when a change in electrical resistivity of a material occurs as a result of applied stress. In other words, piezoresistivity is the change in resistivity of a material as a function of deformation. Germanium [48], silicon [49] and polycrystalline silicon [50] are the most common semiconductor materials that show a piezoresistive effect, and they are frequently used in MEMS for measurement of strain, pressure, acceleration, flow and tactile sensing, as well as haptics applications.

Graphene has attracted a lot of attention, not only due to being the thinnest known material and having unique electrical and mechanical properties, but also due to having a linear change of resistance versus strain, making it a good candidate for piezoresistive sensor applications [51]. In this regard, piezoresistivity of multilayer graphene on poly (methyl methacrylate) (PMMA) substrate was investigated through a bending test that showing high

piezoresistivity with a gauge factor of 50, demonstrating the potential of graphene for strain sensing applications [52]. In addition, Anderson D. Smith et al. verified the piezoresistive effect in graphene by applying uniaxial and biaxial strains [53]. Gauge factors of biaxial strained devices were found to be higher than that of uniaxial ones.

The piezoresistive effect in graphene has been elucidated with three different mechanisms which include: (a) structure deformation, (b) over-connection of graphene sheets, and (c) the tunneling effect among neighboring sheets.

(a) Structure Deformation Electrical-mechanical coupling in graphene can be observed when significant elongation in graphene causes changes in its electrical properties and band structure. Recent studies on strained graphene demonstrate that changes in electrical properties of graphene are related to the type of strain distribution. In symmetrical strain distribution, additional scattering and resistance decrease is observed while no change occurs in other graphene properties such as band-gap opening [54][55][56][57][58][59]. On the other hand, asymmetrical strain distribution in graphene results in opening of band gaps at the Fermi level, which is explained by pseudo-magnetic field. Strain distributions in graphene significantly modify the band structure of graphene around the Fermi level, resulting in remarkable change of the pseudogap width in the case of symmetrical strain distributions and band-gap opening in the case of asymmetrical strain distributions. The band gap is enlarged by increasing the amount of strain, reaching a maximum value of 0.486 eV at 12.2% strain parallel to C-C bonding, and to a maximum of 0.170 eV at 7.3% strain perpendicular to C-C bonding (Figure 1a) [40].

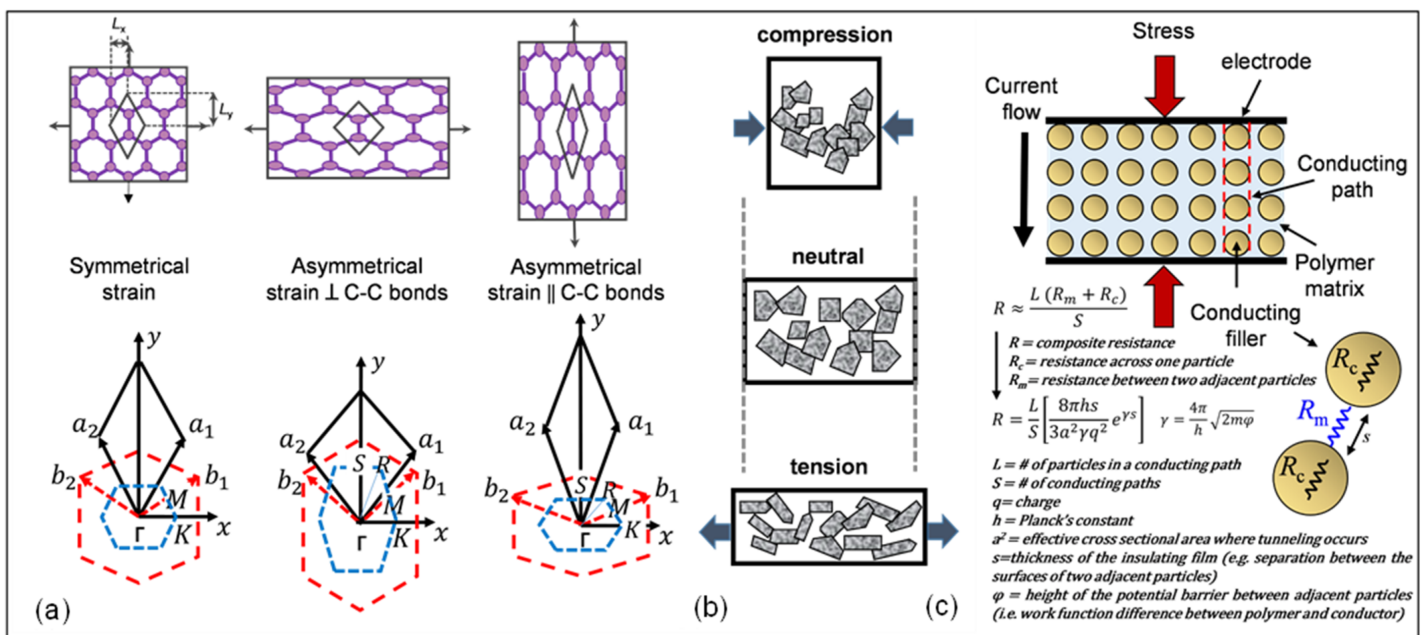


Figure 1. Piezoresistivity mechanisms of graphene: (a) symmetrical strain distribution, asymmetrical strain distribution perpendicular to C-C bonds and asymmetrical strain distribution parallel to C-C bonds [40]; (b) schematic illustration of piezoresistivity of graphene sheets [60]; (c) schematic illustration of the tunneling model.

(b) Over-connected Graphene Sheets As shown in Figure 1b, a larger sheet of graphene can be thought of as a conductive network of smaller connected sheets or flakes. From a nanoscopic perspective, the distortion of a small

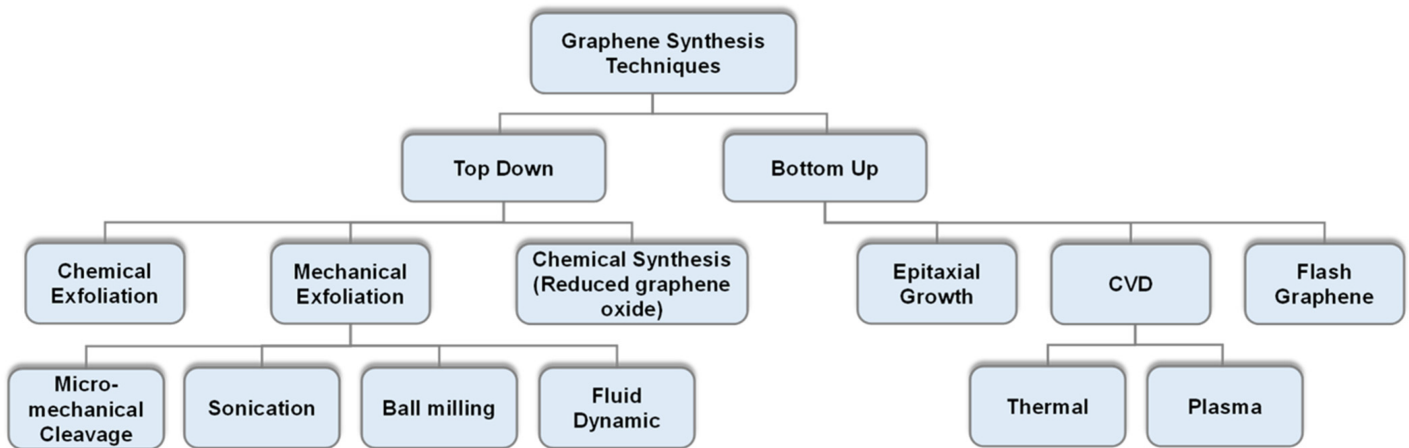
graphene sheet alters the resistivity of the single sheet, which can consecutively trigger a resistance change in the entire conducting system. Thus, the stress response of the graphene network relies primarily on the contact strength of the neighboring plates from a macroscopic point-of-view. Overlap area and contact resistance determine the conductivity between the neighboring flakes. As displayed in **Figure 1b**, the overlap between neighboring flakes becomes smaller or greater such that the resistance changes upon tensile or compressive loading making graphene a suitable material for strain sensing applications [30][60].

(c) Tunneling Effect among Neighboring Graphene Sheets It is known that the distance between two graphene sheets specify the conductivity of graphene. Due to the tunneling effect, current can flow from one single graphene sheet to another. As a result, the resistance increases exponentially and proportionally with the distance (**Figure 1c**) [61]. This mechanism can be used to achieve higher GF in graphene-based strain sensors. As shown in **Figure 1c**, by assuming that the resistance of the matrix is constant everywhere, the resistance of the paths perpendicular to the current flow can be ignored, and thus the number of conducting particles between electrodes, as well as the number of conducting paths, becomes a factor in this relationship. The total resistance can then be calculated as R , which is shown in **Figure 1c**.

3. Methods of Obtaining and Transferring Graphene

Despite its superior electrical and mechanical properties, the challenges in obtaining pristine graphene limit the widespread use of this 2D material in device applications. In an effort to address this problem, numerous techniques were investigated to obtain thin graphitic films and few layer graphene (FLG). Initial demonstrations primarily through mechanical exfoliation followed by transfer of graphene onto silicon substrates, marked a major breakthrough in graphene research [62]. Even though mechanical exfoliation (i.e., Scotch tape method) provides the highest quality graphene, this approach has some disadvantages such as depending largely on the hand skills of the researcher, lack of repeatability and scalability, as well as limitations on graphene flake size and shape being small and irregular.

Therefore, research on obtaining high-quality graphene along with its integration to different substrates which often requires transfer methods, has received serious effort especially over the past two decades. The method with which graphene is obtained directly affects the quality of graphene including its electrical, mechanical and piezoresistive properties. Different methods which are classified as bottom-up and top-down processes have been utilized in order to obtain high-quality graphene. The most commonly used methods are: chemical exfoliation [63], chemical vapor deposition (CVD) [64], epitaxial growth [65], mechanical and reduction of graphene oxide rGO [66][67], and flash graphene synthesis [68]. Graphical overview of these techniques along with the major advantages and drawbacks of each approach are summarized in **Figure 2**.



| Method | Thickness | Lateral | Advantage | Disadvantage |
|--------------------------|------------|----------------------|---|--|
| Chemical Exfoliation | Few layers | nm | High electrical conductivity | Cost of ionic liquids |
| CVD | Few layers | cm | Large size, high quality | Small production scale |
| Epitaxial Growth on SiC | Few layers | up to cm | Very large area of pure graphene | Small production scale |
| Mechanical Exfoliation | Few layers | μm to cm | Large size and unmodified graphene sheets | Very small-scale production |
| Chemical Synthesis (rGO) | Few layers | $< 1 \mu\text{m}$ | Un-oxidized sheets | Contamination with $\alpha\text{-Al}_2\text{O}_3$ and $\alpha\text{-Al}_2\text{S}$ |
| Flash graphene | Few layers | $\sim 1 \mu\text{m}$ | High electrical conductivity | High temperature process |

Figure 2. Overview of the most common techniques to obtain graphene categorized based on top-down and bottom-up processes, along with a tabular comparison on the thickness, lateral size, fundamental advantages and disadvantages of each technique.

4. Graphene-Based Strain Sensors

There are a number of studies in which graphene is used as a strain sensing material. Typically used to fabricate flexible graphene-based strain sensors, graphene can be compounded with elastomers to realize flexible strain sensors with sufficient piezoresistive performance, owing to the excellent electro-mechanical properties of graphene, along with the stretchability and flexibility of polymer matrix. A number of polymers have been utilized in strain sensor applications, where flexibility and stretchability factors are concerned in order to obtain high sensitivity with robust mechanical strength. In this regard, PDMS, PET, 3M elastic adhesive tape, PU and natural rubber have been employed to fabricate graphene-based strain sensors [69].

The performance, more specifically the gauge factor, of these polymer integrated graphene-based strain sensors varies due to different forms of graphene and their implementation methods in polymeric/elastomer matrix structures. We therefore classify graphene strain gauges based on the three most common methods with which graphene is obtained namely: (a) CVD, (b) exfoliation, and (c) reduction of GO. Tabular summary of existing strain

gauges based on the three different forms of graphene is provided in **Table 1**, along with their gauge factor and strain range as performance metrics.

Table 1. Classification of graphene-based strain gauges in terms of the method used to obtain graphene, along with the device topology and performance metrics like gauge factor and strain range.

| Graphene Synthesis Method | Device Topology | Gauge Factor | Strain Range | Ref. |
|---------------------------|--|--------------|--------------|------|
| CVD | RPECVD graphene on mica substrate | 325 | 0.30% | [70] |
| | Graphene-nano graphene sheets on finger | 500 | 1% | [71] |
| | Suspended CVD graphene membrane | 1.6 | 0.25% | [23] |
| | Suspended CVD graphene membrane | 3.67 | 0.29% | [72] |
| | CVD graphene on suspended perforated SiNx membrane | 4.4 | 0.22% | [73] |
| | Graphene glow sensor | 2.4 | 1.8% | [74] |
| | CVD graphene woven fabric on PDMS | 10^6 | 10% | [75] |
| | Graphene-graphene woven on PDMS | 223 | 3% | [76] |
| | Fragmented graphene foam on PDMS | 15–29 | 77% | [77] |
| | Graphene tactile sensor | 1.4 | - | [78] |
| | CVD graphene on PDMS | 6.1 | 1% | [79] |

| Graphene Synthesis Method | Device Topology | Gauge Factor | Strain Range | Ref. |
|---------------------------|--|--------------|--------------|------|
| | braided graphene belts sensor | 175.16 | 55% | [80] |
| | planar and crumpled graphene | 20.1 | 105% | [81] |
| | graphene/g-C ₃ N ₄ heterostructure on PDMS | 1.89 | 25% | [82] |
| | Graphene-single layer graphene on finger | 42.2 | 20% | [26] |
| | Graphene wrapped CNTs | 20 | 1.20% | [83] |
| | PDMS graphene reinforced CNT network | 0.36 | - | [84] |
| Exfoliated graphene | Spray-deposited graphene on a flexible plastic substrate | 10–100 | 1.70% | [85] |
| | Mechanical exfoliated graphene on a silicon wafer | 10–15 | 0.08% | [86] |
| | Mechanical exfoliated graphene nanoribbons | 0.6 | 0.054% | [87] |
| | Mechanical exfoliated graphene nanoribbons | 8.8 | 5% | [88] |
| | Graphene-printed fragments | 125 | 0.30% | [89] |
| | Mechanical exfoliated graphene nanoribbons | 1.9 | 3% | [90] |
| | Graphene solution coated on polypropylene film | 1000 | 0.05–0.265% | [91] |

| Graphene Synthesis Method | Device Topology | Gauge Factor | Strain Range | Ref. |
|---------------------------|---|--------------|--------------|-------|
| | Polymer-functionalized hydrogen-exfoliated graphene | 10 | 0.35% | [92] |
| | Graphene nanoplatelet on PDMS | 62.5 | 2.5–25% | [93] |
| | PDMS-graphene nanoplatelet/CNT hybrids | 1000 | 18% | [94] |
| | Carbon nanotube-graphene nanoplatelet hybrid film | <1 | - | [95] |
| rGO | Mechanical exfoliated Graphene ripple on PDMS | -2 | 20% | [96] |
| | 3D graphene foam-PDMS nanocomposite | 178 | 30% | [97] |
| | rGO on a PET substrate | 61.5 | 0.01–0.04% | [98] |
| | rGO membrane porous structure | 15.2–46.1 | 1% | [99] |
| | PDMS-cellulose-rGO/CNFs hybrids | 9.4 | 70% | [100] |
| | 3D porous PDMS CNT/rGO hybrid | 1.6 | 80% | [101] |
| | Polyurethane-silver nanowires/graphene hybrids | 20–400 | 0.3–1% | [102] |
| | rGO-microtube on PDMS | 630 | 50% | [103] |
| | Crumpled graphene-nanocellulose composite on elastomer matrix | -7.1 | 100% | [104] |

| Graphene Synthesis Method | Device Topology | Gauge Factor | Strain Range | Ref. |
|---------------------------|---|--------------|--------------|-------|
| | rGO doped with polystyrene nanoparticles (PS) on PDMS | 250 | 1.05% | [105] |
| | Polymerized rGO on TPU | 23.15–6583 | 550% | [106] |
| | rGO mesh on an LCP substrate | 375–473 | 0.1–1.4% | [107] |
| | rGO-fish scale like on an elastic tape | 16 | 82% | [108] |
| | rGO-conductive cotton fabric | - | 0.02–0.35% | [109] |
| | rGO-FET on polyethersulfone (PES) | 20 | 50% | [110] |

monitoring and structural health monitoring of polymeric composites. ACS Appl. Mater. Interfaces 2014, 6, 9314–9320.

8. Sun, S.; Han, B.; Jiang, S.; Yu, X.; Wang, Y.; Li, H.; Ou, J. Nano graphite platelets-enabled piezoresistive cementitious composites for structural health monitoring. Constr. Build. Mater. 2017, 136, 314–328.

5.1. Wearable Devices

9. Impson, J.D.; Mehravari, N. Incident-Aware Vehicular Sensors for Intelligent Transportation Systems. U.S. Patent 6,804,602, 12 October 2004.

10. Papadimitratos, P.; De La Fortelle, A.; Evenssen, K.; Brignolo, R.; Cosenza, S. Vehicular communication systems: Enabling technologies, applications, and future outlook on intelligent transportation. IEEE Commun. Mag. 2009, 47, 84–95.

11. Feblemans, S.; Broth, D. Med. J. Servey of Proteins v. C. The Aquilina, P. Science, Use Readings, N. Sensors. The Crisier, P. Application of detecting interest cognitive algorithms to persistent wide area surveillance. In Proc. (EDF) of the 2013 International Conference on Digital Image Computing Techniques and Applications (DICTA), Hobart, Australia, 26–28 November 2013; pp. 1–85, 103 and 106, at strains of 0.2%, 2–6% and >7%, respectively.

12. Berle, F. Multi radar tracking and multi sensor tracking in air defence systems. In Proceedings of the International Radar Symposium, Bangalore, India, 10–13 October 1983; pp. 316–321.

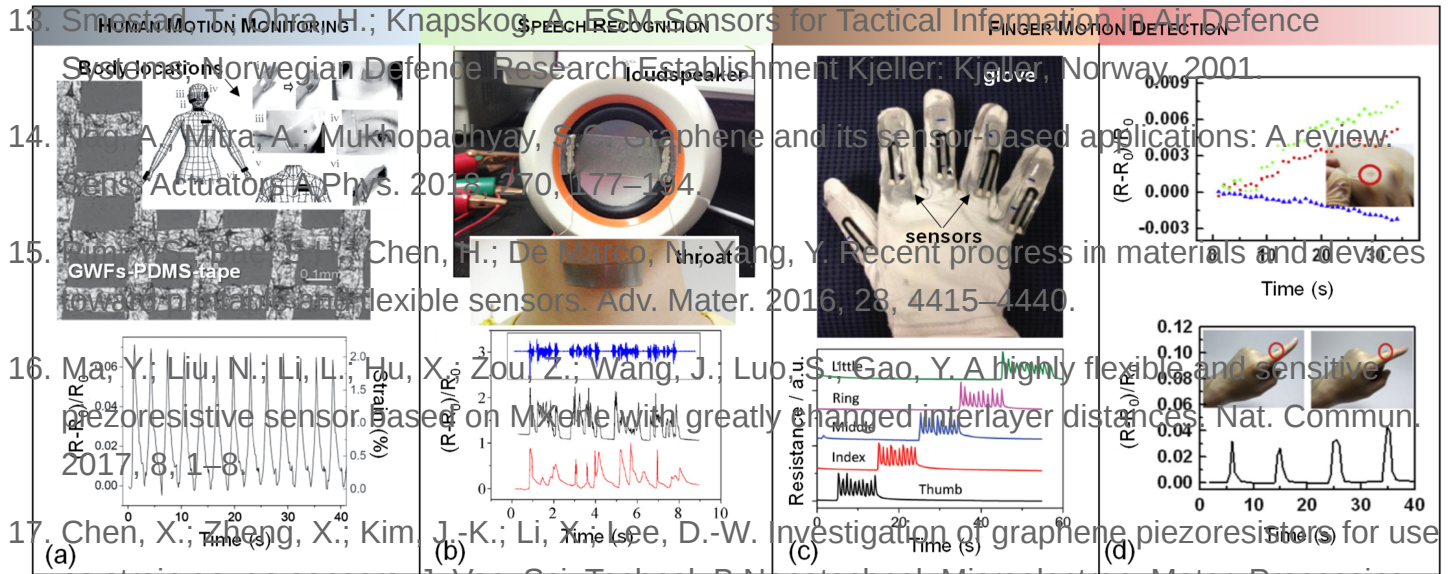


Figure 3. (a) Optical microscope image of graphene woven fabrics (GWFs)-PDMS-tape composite film (scale bar 0.1mm). (b) Graphene-based sensor on a loudspeaker membrane and to a participants' throat, where similar change in relative resistance was observed as the same sentence was played from the loudspeaker (black curve) and read out loud (red curve). (c) Application of graphene nanopaper-based sensors on a glove is imaged and the transitions between the corresponding resistance changes of the strain sensor by the motion of each of the fingers. (d) Observation of relative resistance changes in the strain sensor on a glove when the finger bends or unbends and using a resistive gauge on the glove to detect the direction of principal strain by applying stretch gently.

13. Smestad, T.; Ohra, H.; Knapskog, A. *FSM Sensors for Tactical Information in Air Defence*. Norwegian Defence Research Establishment Kjeller: Kjeller, Norway, 2001.

14. Vora, A.; Mitra, A.; Mukhopadhyay, S. Graphene and its sensor-based applications: A review. *Sens. Actuators A Phys.* 2018, 270, 177–194.

15. Chen, H.; De Marco, M.; Wang, Y. Recent progress in materials and devices flexible sensors. *Adv. Mater.* 2016, 28, 4415–4440.

16. Ma, Y.; Liu, N.; Li, L.; Hu, X.; Zou, Z.; Wang, J.; Luo, S.; Gao, Y. A highly flexible and sensitive piezoresistive sensor based on MXene with greatly changed interlayer distances. *Nat. Commun.* 2017, 8, 1–8.

17. Chen, X.; Zheng, X.; Kim, J.-K.; Li, Y.; Lee, D.-W. Investigation of graphene piezoresistors for use as strain gauge sensors. *J. Vac. Sci. Technol. B Nanotechnol. Microelectron. Mater. Processing Meas. Phenom.* 2011, 29, 06FE01.

18. Singh, A.; Lee, S.; Watababe, H.; Lee, S. Graphene Based Ultra-sensitive Strain Sensors. *ACS Appl. Electron. Mater.* 2020, 2, 523–528.

19. Ma, Z.; Shi, W.; Yan, K.; Pan, L.; Yu, G. Doping engineering of conductive polymer hydrogels and their application in advanced sensor technologies. *Chem. Sci.* 2019, 10, 6232–6244.

20. Wang, X.; Guo, R.; Yuan, B.; Yao, Y.; Wang, F.; Liu, J.; Ni, D. Doped Liquid Metal Printed Highly Stretchable and Conformable Strain Sensor for Multifunctional Human Motion Monitoring. *Proceedings of the 2018 40th Annual International Conference of the IEEE Engineering in Medicine and Biology Society (EMBC), Honolulu, HI, USA, 18–21 July 2018; pp. 3276–3279.*

21. Deroh, M.; Sylvestre, T.; Chretien, J.; Malliotte, H.; Kibler, B.; Beugnot, J.-C. Towards athermal Brillouin strain sensing based on heavily germania-doped core optical fibers. *APL Photonics* 2019, 4, 030801.

22. Liu, Y.; Zhang, D.; Wang, K.; Liu, Y.; Shang, Y. A novel strain sensor based on graphene composite films with layered structure. *Compos. Part A Appl. Sci. Manuf.* 2016, 80, 95–103.

23. Zhu, S.-E.; Krishna Ghatkesar, M.; Zhang, C.; Janssen, G. Graphene based piezoresistive pressure sensor. *Appl. Phys. Lett.* 2013, 102, 161904.

24. Hu, N.; Fukunaga, H.; Atobe, S.; Liu, Y.; Li, J. Piezoresistive strain sensors made from carbon nanotubes based polymer nanocomposites. *Sensors* 2011, 11, 10691–10723.

25. Dresselhaus, M.; Dresselhaus, G.; Saito, R. Physics of carbon nanotubes. *Carbon* 1995, 33, 883–891.

26. Chun, S.; Choi, Y.; Park, W. All-graphene strain sensor on soft substrate. *Carbon* 2017, 116, 753–759.

Technique uses crumpled graphene and nanocellulose. Free-standing flexible nanopapers were created by vacuum filtering, and their 3D structure allowed them to be successfully embedded in an elastomer matrix to produce stretchy nanopapers. However, there is still a restriction about measuring high strains over 50% that are caused by

27. Hossain, D.; Katoji, M.; Mousavi, S.M.; BC9G. Conductive nanocomposite aerogels as a strain over 100 sensor. *Polymer* 2018, **137**, 82–96. A single strain gauge is typically capable of measuring the strain that has the same direction with the position of the gauge. That is why the aligning a strain sensor within the direction of the strain is necessary to obtain an

28. Bøggild, P.; Mackenzie, D.M.; Whelan, P.R.; Petersen, D.H.; Buron, J.D.; Zurutuza, A.; Gallop, J.; Hao, L.; Jepsen, P.U. Mapping the electrical properties of large-area graphene. *2D Mater.* 2017, **4**, 042003.

29. Rapage, D.; G. Kirdocid, A.; Young, R. Intrinsic mechanical properties of graphene and graphene based nanocomposites. *Prog. Mater. Sci.* 2017, **90**, 75–117. Figure 3d illustrates an application onto a

30. Jing, Z.; Guang-Yu, Z.; Dong-Xia, S. Review of graphene-based strain sensors. *Chin. Phys. B* 2013, **22**, 057701.

31. Novoselov, K.S.; Jiang, D.; Schedin, F.; Booth, T.; Khotkevich, V.; Morozov, S.; Geim, A.K. Two-dimensional atomic crystals. *Proc. Natl. Acad. Sci. USA* 2005, **102**, 10451–10453.

32. Zhang, Y.; Tan, Y.-W.; Stormer, H.L.; Kim, P. Experimental observation of the quantum Hall effect and Berry's phase in graphene. *Nature* 2005, **438**, 201–204.

33. Lee, C.; Wei, X.; Kysar, J.W.; Hone, J. Measurement of the elastic properties and intrinsic strength of monolayer graphene. *Science* 2008, **321**, 385–388.

34. Nair, R.R.; Blake, P.; Grigorenko, A.V.; Novoselov, K.S.; Booth, T.J.; Stauber, T.; Peres, N.M.; Geim, A.K. Fine structure constant defines visual transparency of graphene. *Science* 2008, **320**, 1308.

35. Schedin, F.; Geim, A.K.; Morozov, S.V.; Hill, E.; Blake, P.; Katsnelson, M.; Novoselov, K.S. Detection of individual gas molecules adsorbed on graphene. *Nat. Mater.* 2007, **6**, 652–655.

36. Kien, H.W.; Huang, Y.L.; Wang, S.H.; Hsieh, S.H.; Liaw, W.H.; Wang, W.D.; Wang, W.D.; Wang, C.M. Preparation of transparent, conductive resistors by graphene nanosheet application. It yielded a high gauge factor of more than 500 through the control of the ratio of area and resistance. *Chem.* 2012, **22**, 2545–2552.

3.2. Physical Sensors
37. Allen, T. The electronic properties of graphene and carbon nanotubes. *NPG Asia Mater.* 2009, **1**, 17.

38. Allen, M.J.; Tung, V.C.; Kaner, R.B. Honeycomb carbon: A review of graphene. *Chem. Rev.* 2010, **110**, 132–145. Measuring and monitoring the acceleration is vital in various cases such as monitoring activity in biomedical and healthcare applications [121][122], stability control and crash detection in automotive industry [123][124][125], consumer electronics such as cellular phones [1][126], navigation systems, robotic and military applications [127][128][129]. As a

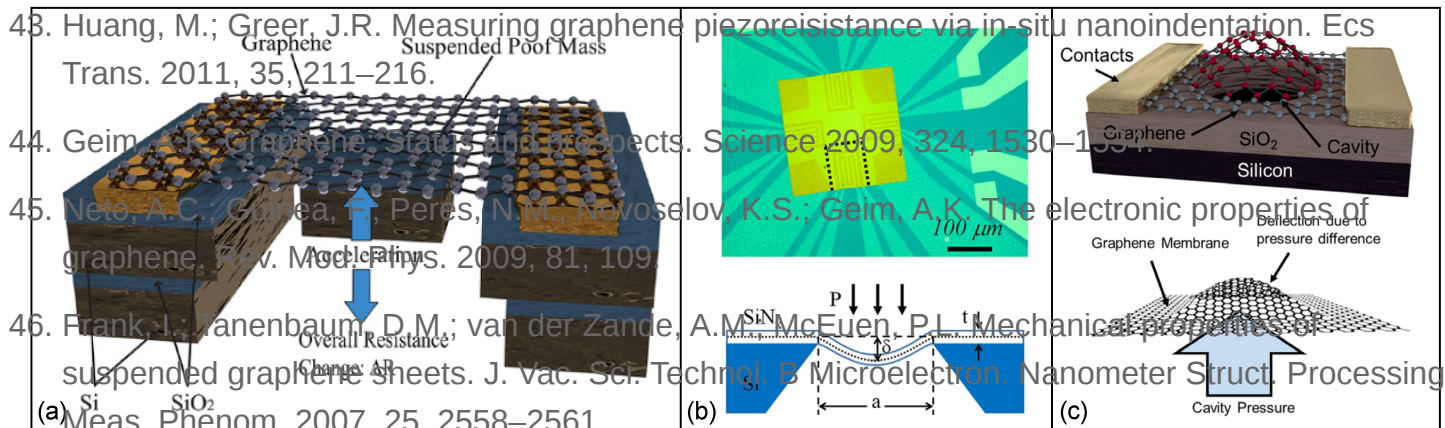
39. Blöchl, K.; Sikes, K.M.; Wang, Z.; Kincaid, M.; Fudenberg, G.; Horvath, G.; Pasztor, H. Amount of deflection in a cantilever mobility suspended graphene. *Solid State Comm.* 2009, **148**, 351–355. A strain high acceleration mobility suspended graphene can be estimated with piezoresistive sensors [130][131].

40. Gui, G.; Li, J.; Zhong, J. Band structure engineering of graphene by strain: First-principles calculations. *Phys. Rev. B* 2008, **78**, 075435.

So far, several studies have reported piezoresistive-based accelerometers employing graphene [132][133][134]. For instance, a piezoresistive transducer was built by using a suspended double-layer graphene ribbon with significant built-in stress (order of 230 to 440 MPa) that shows a noticeable improvement on the static and dynamic

41. Choi, S.-M.; Jhi, S.-H.; Son, Y.-W. Effects of strain on electronic properties of graphene. *Phys. Rev. B* 2010, 81, 081407. the device. Moreover, the device has proof mass that is at least three orders of magnitude less than frequently reported piezoresistive silicon accelerometer proof masses that show a greater magnitude of $\Delta R/R$ per proof mass volume compared to previously reported piezoresistive accelerometers.

42. Sun, L.; Li, Q.; Ren, H.; Su, H.; Shi, Q.; Yang, J. Strain effect on electronic structures of graphene nanoribbons: A first-principles study. *J. Chem. Phys.* 2008, 129, 074704.



43. Huang, M.; Greer, J.R. Measuring graphene piezoresistance via in-situ nanoindentation. *Ecs Trans.* 2011, 35, 211–216.

44. Geim, A.K. Graphene: Status and prospects. *Science* 2009, 324, 1530–1534.

45. Neto, A.C.; Guinea, F.; Peres, N.M.; Novoselov, K.S.; Geim, A.K. The electronic properties of graphene. *Rev. Mod. Phys.* 2009, 81, 109.

46. Frank, J.; Frankenbaum, D.M.; van der Zande, A.M.; McEuen, P.L. Mechanical properties of suspended graphene sheets. *J. Vac. Sci. Technol. B Microelectron. Nanometer Struct. Processing Meas. Phenom.* 2007, 25, 2558–2561.

47. Ovid'ko, I. Mechanical properties of graphene. *Rev. Adv. Mater. Sci.* 2013, 34, 1–11.

48. Shady, S.M.; Frenn, M.; Martin, B. Enhancing the performance of MEMS piezoresistive sensors using germanium nanowire. *Procedia Mater. Sci.* 2015, 16, 254–262.

49. Qin, Y.; Zhao, Y.; Li, Y.; Zhao, Y.; Wang, P. A high performance torque sensor for milling based on a piezoresistive MEMS strain gauge. *Sensors* 2016, 16, 513.

Likewise, graphene-based suspended, planar, spongy and double layer microstructures have been produced as highly flexible and sensitive pressure sensors. Zhu et al. fabricated graphene meandering patterns on silicon nitride membrane. Pressure applied to the graphene membrane caused it to bend and deform into a concave shape in varying degrees. The graphene sensor's piezoresistive effect and out-of-plane deflection allowed

50. Seo, J.-Y. Piezoresistive properties of polycrystalline silicon. *J. Appl. Phys.* 1976, 47, 4780–4783.

51. Khatibi, E. Piezoresistivity of Graphene. Master's Thesis, Politecnico di Milano, Milan, Italy, 2011.

52. Bonaventura, C.; Capressino, A.; Cantaruta, G.; De Nicola, S.; Lapina, A.; Meda, G.; Borgatti, M.; Palomba, M.; Pepe, G.; Valentini, M. Characterization of piezoresistive properties of

graphene-supported polymer coating for strain sensor applications. *Sens. Actuators A Phys.* 2016, 252, 26–34.

Another suspended graphene membrane was fabricated on rectangular and circular cavities (with diameter of 24 μm and depth of 1.5 μm) etched into SiO₂ layer where the membrane was able to deflect due to pressure differences in the sealed cavity and in the pressure chamber. A superior sensitivity in pressure sensing was observed compared to silicon and CNT-based pressure sensors. The maximum GF of the piezoresistive sensor uniaxial and biaxial strain in nanoelectromechanical pressure sensors. *ACS Nano* 2016, 10, 9879–9886.

53. Smith, A.D.; Niklaus, F.; Paussa, A.; Schröder, S.; Fischer, A.C.; Sterner, M.; Wagner, S.; Vaziri, S.; Forsberg, F.; Esseni, D. Piezoresistive properties of suspended graphene membranes under uniaxial and biaxial strain in nanoelectromechanical pressure sensors. *ACS Nano* 2016, 10, 9879–9886.

54. Choi, S.-M.; Jhi, S.-H.; Son, Y.-W. Controlling energy gap of bilayer graphene by strain. *Nano Lett.* 2010, 10, 3486–3489.

55. Cocco, G.; Cadelano, E.; Colombo, L. Gap opening in graphene by shear strain. *Phys. Rev. B* 2010, 81, 241412.

56. Farjam, M.; Rafii-Tabar, H. Comment on “Band structure engineering of graphene by strain: First-principles calculations”. *Phys. Rev. B* 2009, 80, 167401.

57. Jiang, J.-W.; Wang, J.-S. Bright and dark modes induced by graphene bubbles. *EPL (Europhys. Lett.)* 2012, 97, 36004.
58. Lu, Y.; Guo, J. Band gap of strained graphene nanoribbons. *Nano Res.* 2010, 3, 189–199.
59. Pellegrino, F.; Angilella, G.; Pucci, R. Ballistic transport properties across nonuniform strain barriers in graphene. *High Press. Res.* 2012, 32, 18–22.
60. Kim, Y.-J.; Cha, J.Y.; Ham, H.; Huh, H.; So, D.-S.; Kang, I. Preparation of piezoresistive nano smart hybrid material based on graphene. *Curr. Appl. Phys.* 2011, 11, S350–S352.
61. Zhang, X.W.; Pan, Y.; Zheng, Q.; Yi, X.S. Time dependence of piezoresistance for the conductor-filled polymer composites. *J. Polym. Sci. Part B Polym. Phys.* 2000, 38, 2739–2749.
62. Lee, H.C.; Liu, W.-W.; Chai, S.-P.; Mohamed, A.R.; Aziz, A.; Khe, C.-S.; Hidayah, N.M.; Hashim, U. Review of the synthesis, transfer, characterization and growth mechanisms of single and multilayer graphene. *RSC Adv.* 2017, 7, 15644–15693.
63. Bhuyan, M.S.A.; Uddin, M.N.; Islam, M.M.; Bipasha, F.A.; Hossain, S.S. Synthesis of graphene. *Int. Nano Lett.* 2016, 6, 65–83.
64. Li, X.; Cai, W.; An, J.; Kim, S.; Nah, J.; Yang, D.; Piner, R.; Velamakanni, A.; Jung, I.; Tutuc, E. Large-area synthesis of high-quality and uniform graphene films on copper foils. *Science* 2009, 324, 1312–1314.
65. Berger, C.; Song, Z.; Li, X.; Wu, X.; Brown, N.; Naud, C.; Mayou, D.; Li, T.; Hass, J.; Marchenkov, A.N. Electronic confinement and coherence in patterned epitaxial graphene. *Science* 2006, 312, 1191–1196.
66. Hernandez, Y.; Nicolosi, V.; Lotya, M.; Blighe, F.M.; Sun, Z.; De, S.; McGovern, I.; Holland, B.; Byrne, M.; Gun'Ko, Y.K. High-yield production of graphene by liquid-phase exfoliation of graphite. *Nat. Nanotechnol.* 2008, 3, 563.
67. Dreyer, D.R.; Park, S.; Bielawski, C.W.; Ruoff, R.S. The chemistry of graphene oxide. *Chem. Soc. Rev.* 2010, 39, 228–240.
68. Luong, D.X.; Bets, K.V.; Algozeeb, W.A.; Stanford, M.G.; Kittrell, C.; Chen, W.; Salvatierra, R.V.; Ren, M.; McHugh, E.A.; Advincula, P.A. Gram-scale bottom-up flash graphene synthesis. *Nature* 2020, 577, 647–651.
69. Wang, F.; Liu, S.; Shu, L.; Tao, X.-M. Low-dimensional carbon based sensors and sensing network for wearable health and environmental monitoring. *Carbon* 2017, 121, 353–367.
70. Zhao, J.; He, C.; Yang, R.; Shi, Z.; Cheng, M.; Yang, W.; Xie, G.; Wang, D.; Shi, D.; Zhang, G. Ultra-sensitive strain sensors based on piezoresistive nanographene films. *Appl. Phys. Lett.* 2012, 101, 063112.

71. Zhao, J.; Wang, G.; Yang, R.; Lu, X.; Cheng, M.; He, C.; Xie, G.; Meng, J.; Shi, D.; Zhang, G. Tunable piezoresistivity of nanographene films for strain sensing. *ACS Nano* 2015, 9, 1622–1629.
72. Smith, A.; Niklaus, F.; Paussa, A.; Vaziri, S.; Fischer, A.C.; Sterner, M.; Forsberg, F.; Delin, A.; Esseni, D.; Palestri, P. Electromechanical piezoresistive sensing in suspended graphene membranes. *Nano Lett.* 2013, 13, 3237–3242.
73. Wang, Q.; Hong, W.; Dong, L. Graphene “microdrums” on a freestanding perforated thin membrane for high sensitivity MEMS pressure sensors. *Nanoscale* 2016, 8, 7663–7671.
74. Bae, S.-H.; Lee, Y.; Sharma, B.K.; Lee, H.-J.; Kim, J.-H.; Ahn, J.-H. Graphene-based transparent strain sensor. *Carbon* 2013, 51, 236–242.
75. Li, X.; Zhang, R.; Yu, W.; Wang, K.; Wei, J.; Wu, D.; Cao, A.; Li, Z.; Cheng, Y.; Zheng, Q. Stretchable and highly sensitive graphene-on-polymer strain sensors. *Sci. Rep.* 2012, 2, 1–6.
76. Liu, X.; Tang, C.; Du, X.; Xiong, S.; Xi, S.; Liu, Y.; Shen, X.; Zheng, Q.; Wang, Z.; Wu, Y. A highly sensitive graphene woven fabric strain sensor for wearable wireless musical instruments. *Mater. Horiz.* 2017, 4, 477–486.
77. Jeong, Y.R.; Park, H.; Jin, S.W.; Hong, S.Y.; Lee, S.S.; Ha, J.S. Highly stretchable and sensitive strain sensors using fragmented graphene foam. *Adv. Funct. Mater.* 2015, 25, 4228–4236.
78. Park, Y.J.; Lee, S.-K.; Kim, M.-S.; Kim, H.; Ahn, J.-H. Graphene-based conformal devices. *ACS Nano* 2014, 8, 7655–7662.
79. Lee, Y.; Bae, S.; Jang, H.; Jang, S.; Zhu, S.-E.; Sim, S.H.; Song, Y.I.; Hong, B.H.; Ahn, J.-H. Wafer-scale synthesis and transfer of graphene films. *Nano Lett.* 2010, 10, 490–493.
80. Li, Y.; He, T.; Shi, L.; Wang, R.; Sun, J. Strain sensor with both a wide sensing range and high sensitivity based on braided graphene belts. *ACS Appl. Mater. Interfaces* 2020, 12, 17691–17698.
81. Chen, H.; Lv, L.; Zhang, J.; Zhang, S.; Xu, P.; Li, C.; Zhang, Z.; Li, Y.; Xu, Y.; Wang, J. Enhanced stretchable and sensitive strain sensor via controlled strain distribution. *Nanomaterials* 2020, 10, 218.
82. Riyajuddin, S.; Kumar, S.; Gaur, S.P.; Sud, A.; Maruyama, T.; Ali, M.E.; Ghosh, K. Linear piezoresistive strain sensor based on graphene/g-C₃N₄/PDMS heterostructure. *Nanotechnology* 2020, 31, 295501.
83. Eswaraiah, V.; Jyothirmayee Aravind, S.; Balasubramaniam, K.; Ramaprabhu, S. Graphene-Functionalized Carbon Nanotubes for Conducting Polymer Nanocomposites and Their Improved Strain Sensing Properties. *Macromol. Chem. Phys.* 2013, 214, 2439–2444.
84. Shi, J.; Li, X.; Cheng, H.; Liu, Z.; Zhao, L.; Yang, T.; Dai, Z.; Cheng, Z.; Shi, E.; Yang, L. Graphene reinforced carbon nanotube networks for wearable strain sensors. *Adv. Funct. Mater.* 2016, 26, 2078–2084.

85. Hempel, M.; Nezich, D.; Kong, J.; Hofmann, M. A novel class of strain gauges based on layered percolative films of 2D materials. *Nano Lett.* 2012, 12, 5714–5718.
86. Zheng, X.; Chen, X.; Kim, J.-K.; Lee, D.-W.; Li, X. Measurement of the gauge factor of few-layer graphene. *J. Micro/Nanolithogr. MEMS MOEMS* 2013, 12, 013009.
87. Xu, K.; Wang, K.; Zhao, W.; Bao, W.; Liu, E.; Ren, Y.; Wang, M.; Fu, Y.; Zeng, J.; Li, Z. The positive piezoconductive effect in graphene. *Nat. Commun.* 2015, 6, 1–6.
88. Benameur, M.M.; Gargiulo, F.; Manzeli, S.; Autès, G.; Tosun, M.; Yazyev, O.V.; Kis, A. Electromechanical oscillations in bilayer graphene. *Nat. Commun.* 2015, 6, 1–7.
89. Casiraghi, C.; Macucci, M.; Parvez, K.; Worsley, R.; Shin, Y.; Bronte, F.; Borri, C.; Paggi, M.; Fiori, G. Inkjet printed 2D-crystal based strain gauges on paper. *Carbon* 2018, 129, 462–467.
90. Huang, M.; Pascal, T.A.; Kim, H.; Goddard III, W.A.; Greer, J.R. Electronic—Mechanical coupling in graphene from in situ nanoindentation experiments and multiscale atomistic simulations. *Nano Lett.* 2011, 11, 1241–1246.
91. Ismail, Z. Application of Clean & Clear® polymer film as a substrate for flexible and highly sensitive graphene-based strain sensor. *Org. Electron.* 2020, 77, 105501.
92. Sankar, V.; Nambi, A.; Bhat, V.N.; Sethy, D.; Balasubramaniam, K.; Das, S.; Guha, M.; Sundara, R. Waterproof flexible polymer-functionalized graphene-based piezoresistive strain sensor for structural health monitoring and wearable devices. *ACS Omega* 2020, 5, 12682–12691.
93. Baloda, S.; Ansari, Z.A.; Singh, S.; Gupta, N. Development and Analysis of Graphene Nanoplatelets (GNPs)-Based Flexible Strain Sensor for Health Monitoring Applications. *IEEE Sens. J.* 2020, 20, 13302–13309.
94. Zhao, H.; Bai, J. Highly sensitive piezo-resistive graphite nanoplatelet–carbon nanotube hybrids/polydimethylsilicone composites with improved conductive network construction. *ACS Appl. Mater. Interfaces* 2015, 7, 9652–9659.
95. Hwang, S.-H.; Park, H.W.; Park, Y.-B. Piezoresistive behavior and multi-directional strain sensing ability of carbon nanotube–graphene nanoplatelet hybrid sheets. *Smart Mater. Struct.* 2012, 22, 015013.
96. Wang, Y.; Yang, R.; Shi, Z.; Zhang, L.; Shi, D.; Wang, E.; Zhang, G. Super-elastic graphene ripples for flexible strain sensors. *ACS Nano* 2011, 5, 3645–3650.
97. Patole, S.P.; Reddy, S.K.; Schiffer, A.; Askar, K.; Prusty, B.G.; Kumar, S. Piezoresistive and mechanical characteristics of graphene foam nanocomposites. *ACS Appl. Nano Mater.* 2019, 2, 1402–1411.
98. Gamil, M.; Nageh, H.; Bkrey, I.; Sayed, S.; El-Bab, A.M.F.; Nakamura, K.; Tabata, O.; El-Moneim, A.A. Graphene-based strain gauge on a flexible substrate. *Sens. Mater.* 2014, 26, 699–709.

99. Li, J.-C.; Weng, C.-H.; Tsai, F.-C.; Shih, W.-P.; Chang, P.-Z. Porous reduced graphene oxide membrane with enhanced gauge factor. *Appl. Phys. Lett.* 2016, 108, 013108.
100. Wu, S.; Peng, S.; Wang, C.H. Stretchable strain sensors based on PDMS composites with cellulose sponges containing one-and two-dimensional nanocarbons. *Sens. Actuators A Phys.* 2018, 279, 90–100.
101. Chen, M.; Zhang, L.; Duan, S.; Jing, S.; Jiang, H.; Li, C. Highly stretchable conductors integrated with a conductive carbon nanotube/graphene network and 3D porous poly (dimethylsiloxane). *Adv. Funct. Mater.* 2014, 24, 7548–7556.
102. Chen, S.; Wei, Y.; Wei, S.; Lin, Y.; Liu, L. Ultrasensitive cracking-assisted strain sensors based on silver nanowires/graphene hybrid particles. *ACS Appl. Mater. Interfaces* 2016, 8, 25563–25570.
103. Tang, Y.; Zhao, Z.; Hu, H.; Liu, Y.; Wang, X.; Zhou, S.; Qiu, J. Highly stretchable and ultrasensitive strain sensor based on reduced graphene oxide microtubes–elastomer composite. *ACS Appl. Mater. Interfaces* 2015, 7, 27432–27439.
104. Yan, C.; Wang, J.; Kang, W.; Cui, M.; Wang, X.; Foo, C.Y.; Chee, K.J.; Lee, P.S. Highly stretchable piezoresistive graphene–nanocellulose nanopaper for strain sensors. *Adv. Mater.* 2014, 26, 2022–2027.
105. Gong, T.; Zhang, H.; Huang, W.; Mao, L.; Ke, Y.; Gao, M.; Yu, B. Highly responsive flexible strain sensor using polystyrene nanoparticle doped reduced graphene oxide for human health monitoring. *Carbon* 2018, 140, 286–295.
106. Jia, Y.; Yue, X.; Wang, Y.; Yan, C.; Zheng, G.; Dai, K.; Liu, C.; Shen, C. Multifunctional stretchable strain sensor based on polydopamine/reduced graphene oxide/electrospun thermoplastic polyurethane fibrous mats for human motion detection and environment monitoring. *Compos. Part B Eng.* 2020, 183, 107696.
107. Nie, M.; Xia, Y.-h.; Yang, H.-s. A flexible and highly sensitive graphene-based strain sensor for structural health monitoring. *Clust. Comput.* 2019, 22, 8217–8224.
108. Liu, Q.; Chen, J.; Li, Y.; Shi, G. High-performance strain sensors with fish-scale-like graphene-sensing layers for full-range detection of human motions. *ACS Nano* 2016, 10, 7901–7906.
109. Ren, J.; Wang, C.; Zhang, X.; Carey, T.; Chen, K.; Yin, Y.; Torrisi, F. Environmentally-friendly conductive cotton fabric as flexible strain sensor based on hot press reduced graphene oxide. *Carbon* 2017, 111, 622–630.
110. Trung, T.Q.; Tien, N.T.; Kim, D.; Jang, M.; Yoon, O.J.; Lee, N.E. A flexible reduced graphene oxide field-effect transistor for ultrasensitive strain sensing. *Adv. Funct. Mater.* 2014, 24, 117–124.
111. Jang, H.; Park, Y.J.; Chen, X.; Das, T.; Kim, M.S.; Ahn, J.H. Graphene-based flexible and stretchable electronics. *Adv. Mater.* 2016, 28, 4184–4202.

112. Hosseinzadeh, A.; Bidmeshkipour, S.; Abdi, Y.; Arzi, E.; Mohajerzadeh, S. Graphene based strain sensors: A comparative study on graphene and its derivatives. *Appl. Surf. Sci.* 2018, 448, 71–77.
113. Ni, Z.H.; Wang, H.M.; Ma, Y.; Kasim, J.; Wu, Y.H.; Shen, Z.X. Tunable stress and controlled thickness modification in graphene by annealing. *ACS Nano* 2008, 2, 1033–1039.
114. Elias, D.C.; Nair, R.R.; Mohiuddin, T.; Morozov, S.; Blake, P.; Halsall, M.; Ferrari, A.C.; Boukhalov, D.; Katsnelson, M.; Geim, A. Control of graphene's properties by reversible hydrogenation: Evidence for graphane. *Science* 2009, 323, 610–613.
115. Kim, Y.-R.; Bong, S.; Kang, Y.-J.; Yang, Y.; Mahajan, R.K.; Kim, J.S.; Kim, H. Electrochemical detection of dopamine in the presence of ascorbic acid using graphene modified electrodes. *Biosens. Bioelectron.* 2010, 25, 2366–2369.
116. Li, J.; Fang, L.; Sun, B.; Li, X.; Kang, S.H. Recent Progress in Flexible and Stretchable Piezoresistive Sensors and Their Applications. *J. Electrochem. Soc.* 2020, 167, 037561.
117. Boland, C.S.; Khan, U.; Ryan, G.; Barwich, S.; Charifou, R.; Harvey, A.; Backes, C.; Li, Z.; Ferreira, M.S.; Möbius, M.E. Sensitive electromechanical sensors using viscoelastic graphene-polymer nanocomposites. *Science* 2016, 354, 1257–1260.
118. Wang, Y.; Wang, L.; Yang, T.; Li, X.; Zang, X.; Zhu, M.; Wang, K.; Wu, D.; Zhu, H. Wearable and highly sensitive graphene strain sensors for human motion monitoring. *Adv. Funct. Mater.* 2014, 24, 4666–4670.
119. Wang, Y.; Wang, Y.; Yang, Y. Graphene–Polymer Nanocomposite-Based Redox-Induced Electricity for Flexible Self-Powered Strain Sensors. *Adv. Energy Mater.* 2018, 8, 1800961.
120. Wang, Y.; Yang, T.; Lao, J.; Zhang, R.; Zhang, Y.; Zhu, M.; Li, X.; Zang, X.; Wang, K.; Yu, W. Ultra-sensitive graphene strain sensor for sound signal acquisition and recognition. *Nano Res.* 2015, 8, 1627–1636.
121. Del Rosario, M.B.; Redmond, S.J.; Lovell, N.H. Tracking the evolution of smartphone sensing for monitoring human movement. *Sensors* 2015, 15, 18901–18933.
122. Liu, P.S.; Tse, H.-F. Implantable sensors for heart failure monitoring. *J. Arrhythmia* 2013, 29, 314–319.
123. Neul, R.; Gómez, U.-M.; Kehr, K.; Bauer, W.; Classen, J.; Doring, C.; Esch, E.; Gotz, S.; Hauer, J.; Kuhlmann, B. Micromachined angular rate sensors for automotive applications. *IEEE Sens. J.* 2007, 7, 302–309.
124. Fleming, W.J. New automotive sensors—A review. *IEEE Sens. J.* 2008, 8, 1900–1921.
125. Acar, C.; Schofield, A.R.; Trusov, A.A.; Costlow, L.E.; Shkel, A.M. Environmentally robust MEMS vibratory gyroscopes for automotive applications. *IEEE Sens. J.* 2009, 9, 1895–1906.

126. Borgia, E. The Internet of Things vision: Key features, applications and open issues. *Comput. Commun.* 2014, 54, 1–31.
127. Noureldin, A.; Karamat, T.B.; Eberts, M.D.; El-Shafie, A. Performance enhancement of MEMS-based INS/GPS integration for low-cost navigation applications. *IEEE Trans. Veh. Technol.* 2008, 58, 1077–1096.
128. Zhuang, Y.; El-Sheimy, N. Tightly-coupled integration of WiFi and MEMS sensors on handheld devices for indoor pedestrian navigation. *IEEE Sens. J.* 2015, 16, 224–234.
129. Paprotny, I.; Bergbreiter, S. Small-scale robotics: An introduction. In Proceedings of the workshop at the IEEE International Conference on Robotics and Automation, Karlsruhe, Germany, 6–10 May 2013; pp. 1–15.
130. Kazama, A.; Aono, T.; Okada, R. Stress relaxation mechanism with a ring-shaped beam for a piezoresistive three-axis accelerometer. *J. Microelectromech. Syst.* 2012, 22, 386–394.
131. Gesing, A.; Alves, F.; Paul, S.; Cordioli, J. On the design of a MEMS piezoelectric accelerometer coupled to the middle ear as an implantable sensor for hearing devices. *Sci. Rep.* 2018, 8, 1–10.
132. Fan, X.; Forsberg, F.; Smith, A.D.; Schröder, S.; Wagner, S.; Rödjegård, H.; Fischer, A.C.; Östling, M.; Lemme, M.C.; Niklaus, F. Graphene ribbons with suspended masses as transducers in ultra-small nanoelectromechanical accelerometers. *Nat. Electron.* 2019, 2, 394–404.
133. Fan, X.; Forsberg, F.; Smith, A.D.; Schröder, S.; Wagner, S.; Östling, M.; Lemme, M.C.; Niklaus, F. Suspended graphene membranes with attached silicon proof masses as piezoresistive nanoelectromechanical systems accelerometers. *Nano Lett.* 2019, 19, 6788–6799.
134. Hurst, A.M.; Lee, S.; Cha, W.; Hone, J. A graphene accelerometer. In Proceedings of the 2015 28th IEEE International Conference on Micro Electro Mechanical Systems (MEMS), Estoril, Portugal, 18–22 January 2015; pp. 865–868.

Retrieved from <https://encyclopedia.pub/entry/history/show/45113>